Solid Earth Discuss., 7, 1025–1057, 2015
www.solid-earth-discuss.net/7/1025/2015/
doi:10.5194/sed-7-1025-2015

Solid Earth Discussions
Open Access

Structure of the upper mantle in the north-western and central United States from USArray S-receiver functions

R. Kind[1,2], **X. Yuan**[1], **J. Mechie**[1], **and F. Sodoudi**[1]

[1]Deutsches GeoForschungsZentrum Potsdam (GFZ), Potsdam, Germany
[2]Freie Universität, Fachrichtung Geophysik, Berlin, Germany

Received: 10 February 2015 – Accepted: 11 February 2015 – Published: 6 March 2015

Correspondence to: R. Kind (kind@gfz-potsdam.de)

Published by Copernicus Publications on behalf of the European Geosciences Union.

Abstract

We used more than 40 000 S-receiver functions recorded by the USArray project to study the structure of the upper mantle between the Moho and the 410 km discontinuity from the Phanerozoic western United States to the cratonic central US. We obtained clear observations of downward velocity reductions in the uppermost mantle which are commonly interpreted as the lithosphere-asthenosphere boundary (LAB) in the western US and as the mid-lithospheric discontinuity (MLD) in the cratonic US. We observe the western LAB reaching partly to the mid-continental rift system underneath the cratonic crust. The MLD is surprisingly plunging steeply towards the west from the Rocky Mountains Front to about 200 km depth near the Sevier Thrust Belt. There is a significant break in the lithosphere at the Sevier Thrust Belt. We also observe a velocity reduction about 30 km above the 410 km discontinuity in the same region where in the western US the LAB is observed, but not in the cratonic US.

1 Introduction

Lithospheric plates, including thick old cratons, translate over thousands of kilometers over the viscous mantle. However, relatively little is still known about the internal structure of cratons and the transition between the craton and the convecting mantle. Even after more than half a century since the general acceptance of plate tectonic theory, the lithosphere-asthenosphere boundary (LAB) below cratons is still thought to be "elusive" (Eaton et al., 2009) and an additional velocity drop frequently observed in seismic data in the shallow cratonic lithosphere (mid-lithospheric discontinuity, or MLD) is referred to as "enigmatic" (Karato, 2012). These descriptions not only apply to the petrophysical properties of the LAB and MLD but are also a result of still inadequate seismological imaging. The lithosphere-asthenosphere system was originally a mechanical definition (Barrell, 1914) and is not a seismic definition. However, we are using the name LAB here for seismic velocity reductions observed

SED
7, 1025–1057, 2015

near 200 km depth in cratons and near 100 km depth in oceans and Phanerozoic regions by tomography and receiver functions (e.g. Yuan and Romanowicz, 2010). Tomography is not directly sensitive to discontinuities and therefore the transition from lithosphere to asthenosphere is derived from the velocity-depth functions or its vertical gradients (e.g. Yoshizawa, 2014). Only a few tomography studies observed in cratons a shallow low velocity zone near 100 km depth which could be related to the MLD (e.g. Lekic and Romanowicz, 2011).

The alternative view of the deep structure of cratons, independent of the lithosphere-asthenosphere model, defines a tectosphere with the keel of the cratons reaching down to about 400 km (Jordan, 1975). This model is based on different versions of the tomography method (see Jordan and Paulson, 2013 for a recent summary). The tectosphere may be decoupled from the convecting mantle by a low viscosity layer directly above the 410 km discontinuity. A possibly related velocity reduction above the 410 is observed globally by Tauzin et al. (2010).

The LAB and MLD are mainly observed with receiver functions. Summaries of their global distribution are given by Rychert and Shearer (2009), Rychert et al. (2010), Fischer et al. (2010) and Kind et al. (2012). Since the MLD and in some places the cratonic LAB are relatively well observed with seismic body waves, both discontinuities must be relatively sharp. Rychert et al. (2007) deduced from P-receiver functions a sharpness of 11 km for the LAB at the east coast of the US. Li et al. (2007) obtained a sharpness of about 20 km in the western US using S-receiver functions. Rychert et al. (2007) concluded that the sharpness of the LAB excluded temperature variation as the single cause of the LAB. Karato (2012) suggested the grain-boundary sliding model as the cause of the MLD and LAB. This model predicts a strong MLD and weak LAB below cratons. According to Yuan and Romanowicz (2010) the North American craton consists of two layers with different chemistry and anisotropy, with the upper layer reaching to about 100 km depth being the Archean lithosphere. Selway et al. (2015) reviewed the mechanisms which could cause the MLD.

SED
7, 1025–1057, 2015

It would be difficult to show the existence of the MLD in Phanerozoic regions since here the LAB would also be expected at a similar depth. Therefore it is interesting to study the structure of the MLD and LAB at continental collision zones as in the western US. Abt et al. (2010) and Kumar et al. (2012a, b) observed in almost the entire US only a shallow negative discontinuity near 100 km depth. This discontinuity varies to some extent in depth but nowhere does it reach 200 km depth. In the western US and at the east coast this signal was called the LAB while in the central cratonic US it was called the MLD by Abt et al. (2010), and the LAB by Rychert and Shearer (2009) and Kumar et al. (2012a, b). Levander and Miller (2012) have mapped the Phanerozoic LAB in the western US. More detailed regional studies in the western US are published by Rychert et al. (2005, 2007), Li et al. (2007), Hopper et al. (2014), Hansen et al. (2013), Foster et al. (2014) and Lekic and Fischer (2014). Rare observations of the cratonic LAB near about 200 km depth have been obtained by Foster et al. (2014) in the US. Similar observations in other cratons have been obtained in Canada (Miller and Eaton, 2010), Scandinavia (Kind et al., 2013) and South Africa (Sodoudi et al., 2013).

The structure of the mantle lithosphere in western North America was formed by the collision of the Farallon plate with the Laurentia craton and was first resolved by tomographic studies. The subducted Farallon plate is visible in the upper and lower mantle, even below the eastern United States (Grand, 1994; Schmandt and Lin, 2014). The collision with the Precambrian North American craton about 50 million years ago during the Laramide orogeny tore and broke the Farallon plate. An example is the “big break” in the western US of Sigloch et al. (2008) and Sigloch (2011) and references therein, or the vertical high velocity “curtain” near the longitude of Yellowstone (Schmandt and Humphreys, 2011).

2 Methodology

We use the S-receiver function technique (meaning S-to-P conversions) to image seismic discontinuities between the crust-mantle boundary (Moho) and the seismic

SED
7, 1025–1057, 2015

discontinuity at 410 km depth (see e.g. Yuan et al., 2006; Kind et al., 2012 for a description of the technique). The receiver function method determines the response of the Earth structure below a seismic station. Teleseismic waves arriving at a station are scattered by the underlying discontinuities, causing conversions and multiple reflections, which lead to images of the layered structure below the station.

The most important step in receiver function processing is stacking of many seismic traces in order to enhance the weakly converted waves. The simplest approach is to align many records for a given station with respect to a main phase, for example S, after amplitude and sign normalization, and sum these traces. The summation is performed for each component separately (vertical, radial and transverse). We rotated the components by theoretical backazimuth and incidence angle of the S phase and obtained approximately the P, SV and SH response of the medium below the station. As the traveltime moveout between the main phase and the scattered phase depends on epicentral distance, this kind of summation can, without a moveout correction, only be done in narrow epicentral distance windows (Shearer, 1991). A distance moveout correction permits summation over larger distance ranges (Yuan et al., 1997). However, a velocity model is required. Since the moveout correction can only be made for one type of phase at a time (for example P-to-S conversions, or multiples), signals traveling with different slownesses will be canceled by stacking.

Traditionally, deconvolution is used to equalize (and approximately remove) the source signals of the different earthquakes before stacking. For example, in P-receiver functions, a window around the P signal on the vertical component is used to deconvolve the radial component. We should also mention that, theoretically, deconvolution is not required in the receiver function technique. Summation of plain seismograms leads to practically the same results (see Kumar et al., 2010; Bodin et al., 2014). However, the advantages of deconvolution in improving the signal-to-noise ratio prevail. Therefore we apply deconvolution. Another important step in receiver function processing is the migration from the time domain into the depth domain using a known velocity model. For migration, the seismic energy is back-projected along the ray path

SED
7, 1025–1057, 2015

within a given model and stacked, assuming that the energy is distributed in the Fresnel zone (Jones and Phinney, 1998; Kosarev et al., 1999; Yuan et al., 2006). The one dimensional IASP91 reference model is used for moveout correction and migration. Both moveout correction and migration are relatively insensitive to the model used.

We use S-receiver functions in the present study, which have a significant advantage over P-receiver functions for upper mantle studies. In S-receiver functions, the direct conversions arrive before the S signal while the crustal multiples arrive after the S signal. In P-receiver functions, both direct conversions and multiples arrive after the P signal. Multiples in P-receiver functions frequently overwhelm direct conversions and make it difficult to identify the true structure. However, S-receiver functions have other problems which need to be considered. In the next section we include a discussion of some problems of the interpretation of the wave field of S precursors using the example of USArray data.

3 Data

We obtained the data from the open access IRIS archive in Seattle, Washington (www.iris.edu). Most data are provided by the USArray project (www.usarray.org), which is a continent-wide temporary mobile network with a spacing of about 70 km between stations. The locations of the seismic stations used in this study are shown in Fig. 1. The distribution of the epicenters of the earthquake records used is shown in Fig. 2. We have inspected manually over 200 000 records from events with magnitudes greater than 5.7 within the epicentral distance range of 60–85°. Conditions for the selection of traces were a signal-to-noise ratio of at least two in the original broadband S signal on the SV component, a good approximation of a spike by the deconvolved SV signal, low energy at the time of the spike on the P component and no obviously disturbing signals before the S arrival on the P component. This procedure appears to be robust, since several persons participated in selecting data along these lines without a visible personal influence.

SED
7, 1025–1057, 2015

Finally more than 40 000 records have been selected for our study. Next we will discuss the wave field of the S precursors of all available data in different graphical presentations. All data in the following figures are lowpass filtered with 8 s corner period. In Fig. 3a all traces are shown as a function of the epicentral distance. The traces are summed within 0.5° windows of epicentral distance disregarding the backazimuth and station location. The same data are shown in Fig. 4 as common conversion point (CCP) stacks and as a function of the station locations. Distance (or slowness) moveout corrected traces (reference slowness 6.4 s per degree) are summed, with hypothetical S-to-P piercing points at 200 km depth within a certain geographical box. The back azimuth is disregarded. The boxes are aligned along west–east and south–north profiles. West–east profiles are shown in Fig. 4a. The box size is 0.5° longitude and extends in the south–north direction over the entire array. South–north profiles are shown in Fig. 4b. The box size is 1° latitude and extends in west–east direction also over the entire array. In Fig. 5 the traces are shown from the cratonic part of the network (east of 110° W longitude) as a function of the backazimuth. There is no overlapping of windows. Neighboring stacked traces therefore do not contain any common traces.

There are obviously several seismic phases visible in Figs. 3–5. Seismic phases marked red (positive) are caused by a discontinuity with downward increasing velocity. Blue phases (negative) mark downward decreasing velocity. All phases converted from the direct S phase to P are marked with black labels in Figs. 3–5. These are the conversions from the Moho, two blue phases labeled LVZ1 and LVZ2, the conversion from the discontinuity at 410 km depth (marked “410”), a red discontinuity marked “Lehmann” and another blue discontinuity following closely the 410 signal and marked “LVZ410”. The Moho is not the focus of our study. The LVZ410 is observed in P- and S-receiver functions by a number of authors in different parts of the world (e.g. by Schaeffer and Bostock, 2010 in northwestern Canada; by Vinnik et al., 2010 in California and globally by Tauzin et al., 2010). It is interpreted by the presence of water causing partial melt. Jordan and Paulson (2013) discuss the role of this discontinuity

SED
7, 1025–1057, 2015

for decoupling the thick continental tectosphere (which extends below the LAB) from the convecting mantle. The Lehmann discontinuity is widely considered as the bottom of the asthenosphere. A global study of the Lehmann discontinuity given by Gu et al. (2001).

Theoretical traveltime curves of S precursors at the above mentioned discontinuities are marked by dashed black lines in Fig. 3a. They are computed using the IASP91 global reference model with three negative discontinuities (LVZ1, LVZ2 and LVZ410 at 90, 170 and 380 km depth, respectively) and one positive discontinuity (Lehmann at 270 km) added. The Moho is set at 35 km depth. LVZ1 and the 410 are clearly observed in Figs. 3–5. The LVZ2 and the Lehmann discontinuity are better observed in Fig. 4.

Additional seismic phases, besides the ones discussed so far are only visible in Fig. 3a but not in Figs. 4 and 5. Theoretical traveltime curves have been computed to explain these phases. They are marked in green. We see clear negative SKS660p and ScS660p phases from the 660 km discontinuity cutting through all other phases prior to the S arrival. These phases are strong at 68–73 and 75–79° epicentral distances and 10–30 s precursor time, and at 75–80° epicentral distance and 40–50 s precursor time, where they cut through the LVZ2 and the LVZ410 signals. However, the signals are caused by the SKS and ScS conversions at the 410 and 660 discontinuities and have very different slownesses than the S phase. This is the reason why they are canceled out in the moveout corrected and stacked signals in Figs. 4 and 5. There are also surprisingly clear phases after the S signal in Fig. 3a. They are the crustal multiples SsPmp and SPn below the stations (see the ray path of SPn in Fig. 3b), which are so far not much used to infer information about the P velocity below the stations.

There have been concerns that higher order P multiples could influence S precursors on the P component (Bock, 1994; Wilson et al., 2006). However, we do not see such phases in the complete observed precursor wave field in Fig. 3a. The reason is probably that the upper mantle of the Earth is too heterogeneous to permit the efficient propagation of higher order P multiples. In Fig. 6 we have computed S precursors for the one dimensional IASP91 Earth model (vertical component). We used the version

SED
7, 1025–1057, 2015

of the reflectivity method by Kind (1985), which is an extension of the original method by Fuchs and Müller (1971) for different source and receiver structures. This version avoids P multiples in the theoretical seismograms, which cause a high noise level in front of the S phase making it difficult to get good S precursors. An approximated spike was used as the source time function. The strong SPn and SsPmp phases after S agree well with the data in Fig. 3a. A disagreement between computed and observed seismograms is the source-side Pn in front of the S signal (Fig. 6), which is not in the data (Fig. 3a). This is a phase traveling as P along the surface on the source side and continuously radiating S waves downward. At the receiver side these phases are converted back to P and travel again horizontally along the surface. These phases are not observed in the stacked S-receiver functions (Fig. 3a) because of stacking of records from many regions with different structures and source depths. The same phases marked green in the data (Fig. 3a) are also marked green in the theoretical seismograms in Fig. 6. Note that the IASP91 model does not have an upper mantle low velocity zone, nor the Lehmann discontinuity and also not the negative discontinuity above the 410. Therefore these phases are not computed.

In order to point out another possible source of disturbing S precursors, we have computed theoretical seismograms similar to Fig. 6 for different crustal models at the source and receiver sides (see Fig. 7). A narrower slowness integration window was used, which excludes source-side Pn. There is a 50 km thick crust at the source side in Fig. 7a and no crust is included at the source side in Fig. 7b. Receiver-side crust is in both cases 40 km thick. The rotated L component is shown, which carries practically only P energy. We see ScS and SKS conversions at the 410 and 660 discontinuities, which cross the Sp conversions at the Moho and at the 410. In Fig. 7c ray paths of Smp with a conversion at the receiver-side Moho (Fig. 7b) and of PmSmp with an additional P-to-S conversion at the source-side Moho (Fig. 7a) are shown. The PmSmp phase is visible in Fig. 7a as a negative precursor of the Moho conversion, which might be mistaken in the real data as a S-to-P conversion at a negative discontinuity below the Moho underneath the station. In receiver functions, however, this phase is reduced due

SED
7, 1025–1057, 2015

to summation of many events with different source depths and source-side structures. Care should be taken if single seismograms are used because it seems impossible to identify all phases uniquely in these cases.

4 Topography of MLD and LAB

To image the topography of the LAB and MLD in the study area we plotted in Fig. 8 narrow west–east profiles with the receiver functions migrated into the depth domain. The width of each profile is 2° latitude with 1° overlap. The IASP91 model is used for migration. In the uppermost mantle below the Moho we observe two clearly correlatable blue signals (velocity decrease downward) marked with dashed lines. These phases agree well with known signals from the LAB in the western US (dashed magenta line) and the MLD in the central US (dashed yellow line). North of about 46° N the LAB dips gradually from near 100 km depth at the west coast to about 200 km depth near 90° W at the mid-continental rift system (MCRS), where it ends abruptly. The gradually dipping LAB extends further to the east underneath the craton than the tomographic Farallon slab as suggested e.g. by Bunge and Grand (2000). Between about 39 and 46° N the LAB remains near 100 km depth and ends abruptly at 110–112° W. In the same latitude range the MLD dives to the west from near 100 km depth below the cratonic US to about 200 km depth at 110–112° W. There is a relatively sharp step at this longitude range from the shallow LAB in the west to the deep MLD in the east. South of about 39° N the LAB appears very similar to the LAB north of about 46° N. However, the signals are weaker in the south than in the north. To highlight the differences in the LAB and MLD topography between these three regions, we show one profile for each of these three regions in Fig. 9a–c. Comparing the location of the observed LAB and MLD structure with surface geology, we find that the big break in the lithosphere observed in Fig. 9b extends roughly from the Yellowstone region to the Colorado Plateau along the Sevier Thrust Belt (see Fig. 1). In this region the MLD is flat and at normal shallow depths east of the Rocky Mountains front and steeply west-dipping between the Rocky Mountains

SED
7, 1025–1057, 2015

front and the Sevier Thrust Belt. North of 46° N and south of 39° N the east-dipping LAB of the western US extends to the mid-continental rift system (Fig. 9a and c).

How do our observations agree with earlier seismic images of the mantle lithosphere in the western and central US? Levander and Miller (2012) also used S-receiver function data from USArray in the same area. They also observe the break in the LAB along the Sevier Thrust Belt. However they interpret the deep velocity drop east of the Sevier Thrust Belt as the cratonic LAB of the Laurentia plate. They do not report on the MLD and a west-dipping structure between the Rocky Mountains front and the Sevier Thrust Belt. Hopper et al. (2014) observed in the Yellowstone region the same break in the mantle lithosphere, also using S-receiver functions. They observed east of Yellowstone a faint shallow MLD but no west-dipping structure. Hansen et al. (2013) observed the LAB below the Colorado Plateau at 100–150 km depth and east of it at 150 to 200 km depth. This agrees with our LAB observations along 38° N (Fig. 8l). Foster et al. (2014) also studied the lithosphere in the American Midwest with USArray S-receiver functions. They observed east of about 98° W a strong MLD near 100 km depth and the cratonic LAB at 200–250 km depth. Their data are close to our profile shown in Fig. 8d. We also see here a strong MLD east of about 98° W. However we see, in addition, indications of the east-dipping LAB and the west-dipping MLD within the 2° latitude wide profile in Fig. 8d. Lekic and Fischer (2014) observed below the Colorado Plateau and surroundings scattered negative signals near 100 km depth in S-receiver functions which they interpreted as the LAB beneath the Basin and Range Province and the Rocky Mountains front, west and east of the Colorado Plateau, respectively. Beneath the stable Colorado Plateau and the Great Plains they interpreted a negative phase in the same depth range as the MLD. We observe mainly below the Colorado Plateau the east-dipping LAB of the western US at 100–150 km depth (Fig. 9c). However, this signal is not as strong as the equivalent signal north of Yellowstone.

Figure 9d–g shows four south–north profiles. In the westernmost profile (Fig. 9d) only the LAB is observed. The next profile to the east (Fig. 9e) shows in the south and in the north the LAB. However, in the center it shows the MLD which is plunging to

SED
7, 1025–1057, 2015

the west here. In the easternmost two profiles (Fig. 9f and g) we see the MLD with the cratonic LAB underneath. Our observations of the cratonic LAB indicate, together with other S-receiver function observations (Miller and Eaton, 2010 in Canada and Kind et al., 2013 in Scandinavia), that the deep cratonic LAB is visible in converted waves, which is evidence for its sharpness. A study of the complete USArray data in the east is required for a more comprehensive analysis of the cratonic LAB. Close to the east coast the LAB again seems to occur near 100 km depth (Rychert et al., 2007).

5 Anisotropy of the MLD?

Sodoudi et al. (2013) found in South Africa MLD signals in S receiver functions showing azimuthal anisotropy. They observed a sign change of the S-to-P converted signal from about 85 km depth with a periodicity of 180° backazimuth. The MLD in our data does not show any sign change or significant change of the amplitudes as a function of the backazimuth (see LVZ1 in Fig. 5). This means that there are no indications in our data for azimuthal anisotropy as the cause of the MLD signal in the cratonic US. This seems to be in contradiction to the anisotropy model obtained from a joint inversion of tomography and SKS data (Yuan and Romanowicz, 2010).

6 Low velocity zone above the 410 km discontinuity

Tauzin et al. (2010) observed a nearly global velocity reduction at about 350 km depth without any relation to surface tectonics. The cause of this low velocity layer is thought to be partial melt caused by dehydration (Bercovici and Karato, 2003). We observed a similar discontinuity in the USArray S-receiver functions (see e.g. Figs. 4 and 9). Jordan and Paulson (2013) suggested that a low viscosity zone directly above the 410 discontinuity decouples the thick cratonic tectosphere from the flowing mantle. Looking at Figs. 4 and 9 we see that the strongest signals of the phase LVZ410 are observed in the western US where the LAB occurs at about 100 km depth. The

SED
7, 1025–1057, 2015

signal is weak or non-existent in the cratonic US. This means that the velocities directly above the 410 are lower in Phanerozoic regions than in cratonic regions. This supports the tomographic results summarized by Jordan and Paulson (2013) of the cratonic tectosphere reaching down to the 410 km discontinuity.

7 Conclusions

We have been able to image with S-receiver functions the major seismic discontinuities in the upper mantle below large regions of the western and central United States. In the upper 200 km we see complicated structures of the western LAB and the central MLD (Fig. 10). The east-dipping LAB interferes with the west plunging MLD in a complicated manner. We interpret these structures as being caused by the continental collision of the Farallon plate and the Laurentia plate (Fig. 1). The MLD appears to be deformed in this collision in a similar way as could be expected for a shallow non-cratonic LAB. This could mean that the Archean lithosphere of the craton (Yuan and Romanowicz, 2010) was deformed during the collision with the Farallon plate. The western LAB dips gradually far to the east to the mid-continental rift system, where it could be mistaken for the cratonic LAB. The deep cratonic LAB near 200 km depth is only weakly observed at the eastern end of the considered area (from about 90 to 82° W). Its connection to the previously observed shallow LAB near the Atlantic coast needs further investigation with all eastern USArray data. Below 200 km depth we have observed a scattered Lehmann discontinuity, which is considered to be the bottom of the asthenosphere. Directly above the 410 km discontinuity mainly in the western US we observed a strong velocity reduction. Such a velocity reduction directly above the 410 is not observed in the cratonic US, which indicates higher velocity here. This observation is in agreement with the model of the cratonic tectosphere reaching to the 410 km discontinuity.

Acknowledgements. This research was supported by the Deutsche Forschungsgemeinschaft. The facilities of the IRIS Data Management System, and specifically the IRIS Data Management Center, were used for access to waveform and metadata required in this study

SED
7, 1025–1057, 2015

(http://ds.iris.edu/data/). The IRIS DMS is funded through the National Science Foundation and specifically the GEO Directorate through the Instrumentation and Facilities Program of the National Science Foundation under Cooperative Agreement EAR-1063471. We also wish to thank Gene Humphreys and Shun Karato for discussions, and Theresia Ziegs and Irene Kind for help in the data processing.

The article processing charges for this open-access publication have been covered by a Research Centre of the Helmholtz Association.

References

Abt, D. L., Fischer, K. M., French, S. W., Ford, H. A., Yuan, H., and Romanowicz, B.: North American lithospheric discontinuity structure imaged by Ps and Sp receiver functions, J. Geophys. Res., 115, B09301, doi:10.1029/2009JB006914, 2010.

Barrell, J.: The strength of the Earth's crust, J. Geol., 22, 655–683, 1914.

Bercovici, D. and Karato, S.: Whole mantle convection and transition-zone water filter, Nature, 425, 39–44, 2003.

Bock, G.: Multiples as precursors to S, SKS and ScS, Geophys. J. Int., 119, 421–427, 1994.

Bodin, Th.,Yuan, H., and Romanowicz, B.: Inversion of receiver functions without deconvolution-application to the Indian craton, Geophys. J. Int., 196, 1025–1033, doi:10.1093/gji/ggt431, 2014.

Bunge, H.-P. and Grand, S. P.: Mesozoic plate-motion history beneath the northeast Pacific ocean from seismic images of the subducted Farallon slab, Nature, 405, 337–340, 2000.

Eaton, D. W., Darbyshire, F., Evans, R. L., Grütter, H., Jones, A. G., and Yuan, X.: The elusive lithosphere–asthenosphere boundary (LAB) beneath cratons, Lithos, 109, 1–22, doi:10.1016/j.lithos.2008.05.009, 2009.

Foster, K., Dueker, K., Schmandt, B., and Yuan, H.: A sharp cratonic lithosphere–asthenosphere boundary beneath the American Midwest and its relation to mantle flow, Earth Planet. Sc. Lett., 402, 82–89, 2014.

Fischer, K. M., Ford, H. A., Abt, D. L., and Rychert, C. A.: The lithosphere–asthenosphere boundary, Annu. Rev. Earth Pl. Sc., 38, 551–575, doi:10.1146/annurev-earth-040809-152438, 2010.

SED
7, 1025–1057, 2015

Fuchs, K. and Müller, G.: Computation of synthetic seismograms with the reflectivity method and comparison with observations, Geophys. J. Int., 23, 417–433, doi:10.1111/j.1365-246X.1971.tb01834.x, 1971.
Grand, S.: Mantle shear structure beneath the Americas and surrounding oceans, J. Geophys. Res., 99, 11591–11621, 1994.
Gu, J. Y., Dziewonski, A. M., and Ekström, G.: Preferential detection of the Lehmann discontinuity beneath continents, Geophys. Res. Lett., 28, 4655–4658, 2001.
Hansen, S., Dueker, K., Stachnik, J., Aster, R., and Karlstrom, K. A.: A rootless rockies – support and lithospheric structure of the Colorado Rocky Mountains inferred from CREST and TA seismic data, Geochem. Geophy. Geosy., 14, 2670–2695, doi:10.1002/ggge.20143, 2013.
Hopper, E., Ford, H. E., Fischer, K. M., and Lekic, V.: The lithosphere-asthenosphere boundary and the tectonic-magmatic history of the northwestern United States, Earth Planet. Sc. Lett., 402, 69–81, 2014.
Jones, C. H. and Phinney, R. A.: Seismic structure of the lithosphere from teleseismic converted arrivals observed at small arrays in the southern Sierra Nevada and vicinity, California, J. Geophys. Res., 103, 10065–10090, doi:10.1029/97JB03540, 1998.
Jordan, T. H.: The continental tectosphere, Rev. Geophys. Space Ge., 13, 1–12, 1975.
Jordan, T. H. and Paulson, E. M.: Convergence depths of tectonic regions from an ensemble of global tomographic models, J. Geophys. Res.-Sol. Ea., 118, 4196–4225, doi:10.1002/jgrb.50263, 2013.
Karato, S.: The origin of the asthenosphere, Earth Planet. Sc. Lett., 321–322, 95–103, doi:10.1016/j.epsl.2012.01.001, 2012.
Kind, R.: The reflectivity method for different source and receiver structures, J. Geophys., 58, 146–152, 1985.
Kind, R., Yuan, X., and Kumar, P.: Seismic receiver functions and the lithosphere-asthenosphere boundary, Tectonophysics, 536–537, 25–43, doi:10.1016/j.tecto.2012.03.005, 2012.
Kind, R., Sodoudi, F., Yuan, X., Shomali, H., Roberts, R., Gee, D., Eken, T., Bianchi, M., Tilmann, F., Balling, N., Jacobsen, B. H., Kumar, P., and Geissler, H. W.: Scandinavia: a former Tibet?, Geochem. Geophy. Geosy., 14, 4479–4487, doi:10.1002/ggge.20251, 2013.

SED
7, 1025–1057, 2015

Kosarev, G., Kind, R., Sobolev, S. V., Yuan, X., Hanka, W., and Oreshin, S.: Seismic evidence for detached Indian lithospheric mantle beneath central Tibet, Science, 283, 1306–1308, 1999.

Kumar, P., Kind, R., and Yuan, X. H.: Receiver function summation without deconvolution, Geophys. J. Int., 180, 1223–1230, doi:10.1111/j.1365-246X.2009.04469.x, 2010.

Kumar, P., Yuan, X., Kind, R., and Mechie, J.: The lithosphere-asthenosphere boundary observed with USArray receiver functions, Solid Earth, 3, 149–159, doi:10.5194/se-3-149-2012, 2012a.

Kumar, P., Kind, R., Yuan, X., and Mechie, J.: USArray receiver function images of the LAB, Seismol. Res. Lett., 83, 486–491, doi:10.1785/gssrl.83.3.486, 2012b.

Levander, A. and Miller, M. S.: Evolutionary aspects of lithosphere discontinuity structure in the western US, Geochem. Geophy. Geosy., 13, Q0AK07, doi:10.1029/2012GC004056, 2012.

Lekic, V. and Fischer, K.: Contrasting lithospheric signatures across the western United States revealed by Sp receiver functions, Earth Planet. Sc. Lett., 42, 90–98, doi:10.1016/j.epsl.2013.11.026, 2014.

Lekic, V. and Romanowicz, B.: Tectonic regionalization without a priori information: a cluster analysis of upper mantle tomography, Earth Planet. Sc. Lett., 308, 151–160, doi:10.1016/j.epsl.2011.05.050, 2011.

Li, X., Yuan, X. H., and Kind, R.: The lithosphere–asthenosphere boundary beneath the western United States, Geophys. J. Int., 170, 700–710, doi:10.1111/j.1365-246X.2007.03428.x, 2007.

Miller, M. S. and Eaton, D. W.: Formation of the cratonic mantle keels by accreation: evidence from S receiver functions, Geophys. Res. Lett., 37, L18305, doi:10.1029/2010GL044366, 2010.

Rychert, C., Fischer, K., and Rondenay, S. A.: A sharp lithosphere–asthenosphere boundary imaged beneath eastern North America, Nature, 436, 542–547, doi:10.1038/nature03904, 2005.

Rychert, C. A. and Shearer, P. M.: A global view of the lithosphere-asthenosphere boundary, Science, 324, 495–498, 2009.

Rychert, C. A., Shearer, P. M., and Fischer, K. M.: Scattered wave imaging of the lithosphere–asthenosphere boundary, Lithos, 120, 173–185, doi:10.1016/j.lithos.2009.12.006, 2010.

SED
7, 1025–1057, 2015

Rychert, K., Rondenay, S., and Fischer, K.: P-to-S and S-to-P imaging of a sharp lithosphere–asthenosphere boundary beneath eastern NorthAmerica, J. Geophys. Res., 112, B08314, doi:10.1029/2006jb004619, 2007.
Schaeffer, A. J. and Bostock, M. G.: A low-velocity zone atop the transition zone in northwestern Canada, J. Geophys. Res., 115, B06302, doi:10.1029/2009JB006856, 2010.
Schmandt, B. and Humphreys, E.: Seismically imaged relict slab from the 55 Ma Siletzia accretion to the northwest United States, Geology, 39, 175–178, doi:10.1130/G31558.1, 2011.
Schmandt, B. and Lin. F.-C.: P and S wave tomography of the mantle beneath the United States, Geophys. Res. Lett., 41, 6342–6349, doi:10.1002/2014GL061231, 2014.
Selway, K., Ford, H., and Kelemen, P.: The seismic mid-lithospheric discontinuity, Earth Planet. Sc. Lett., 414, 45–57, doi:10.1016/j.epsl.2014.12.029, 2015.
Shearer, P. M.: Constraints on upper mantle discontinuities from observations of long-period reflected and converted phases, J. Geophys. Res., 96, 18147–18182, 1991.
Sigloch, K.: Mantle provinces under North America from multifrequency P wave tomography, Geochem. Geophy. Geosy., 12, Q02W08, doi:10.1029/2010GC003421, 2011.
Sigloch, K., McQuarrie, N., and Nolet, N.: Two-stage subduction history under North America inferred from multiple-frequency tomography, Nat. Geosci., 1, 458–462, doi:10.1038/ngeo231, 2008.
Sodoudi, F., Yuan, X., Kind, R., Lebedev, S., Adam, J. M.-C., Kästle, E., and Tilmann, F.: Seismic evidence for stratification in composition and anisotropic fabric within the thick lithosphere of Kalahari Craton, Geochem. Geophy. Geosy., 14, 5393–5412, doi:10.1002/2013GC004955, 2013.
Tauzin, B., Debayle, E., and Wittlinger, G.: Seismic evidence for global low-velocity layer within the Earth's upper mantle, Nat. Geosci., 3, 718–721, doi:10.1038/NGEO969, 2010.
Vinnik, L., Ren, Y., Stutzmann, E., Farra, V., and Kiselev, S.: Observations of S410p and S350p phases at seismograph stations in California, J. Geophys. Res., 115, B05303, doi:10.1029/2009JB006582, 2010.
Wilson, D. C., Angus, D. A., Ni, J. F., and Grand, S. P.: Constraints on the interpretation of S-to-P receiver functions, Geophys. J. Int., 165, 969–980, 2006.
Yoshizawa, K.: Radially anisotropic 3-D shear wave structure of the Australian lithosphere and asthenosphere from multi-mode surface waves, Phys. Earth Planet. In., 235, 33–48, doi:10.1016/j.pepi.2014.07.008, 2014.

SED
7, 1025–1057, 2015

Yuan, H. Y. and Romanowicz, B.: Lithospheric layering in the North American craton, Nature, 466, 1063–1071, doi:10.1038/nature09332, 2010.

Yuan, X., Ni, J., Kind, R., Mechie, J., and Sandvol, E.: Lithospheric and upper mantle structure of southern Tibet from a seismological passive source experiment, J. Geophys. Res., 102, 27491–27500, 1997.

Yuan, X., Kind, R., Li, X., and Wang, R.: The S receiver functions; synthetics and data example, Geophys. J. Int., 165, 555–564, doi:10.1111/j.1365-246X.2006.02885.x, 2006.

SED

7, 1025–1057, 2015

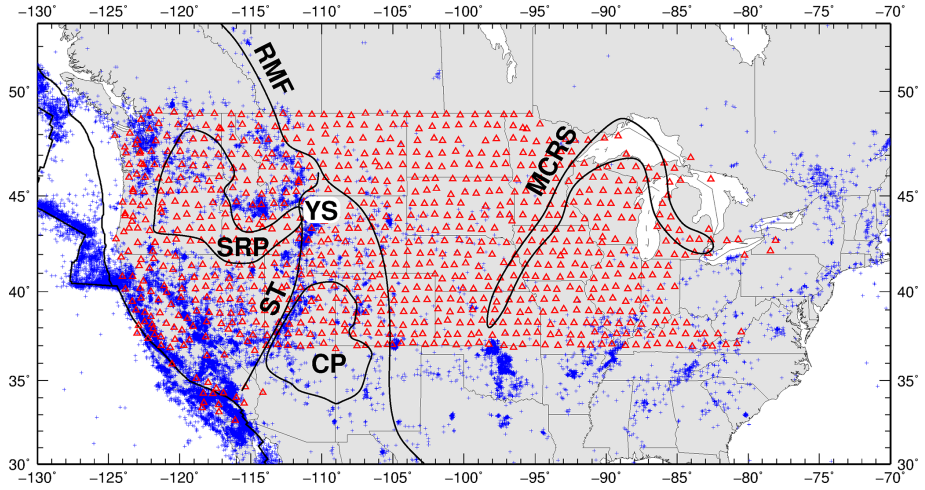

Figure 1. Map of North America with seismic stations (triangles) from USArray (http://www.usarray.org/researchers/obs/transportable), the Berkeley seismic network (https://seismo.berkeley.edu), the Southern California network (http://www.scsn.org), and the permanent network of the US Geological Survey (http://earthquake.usgs.gov/monitoring/anss/). The data have been obtained from the IRIS data archive (http://ds.iris.edu/data/). Seismicity (blue crosses) and relevant geological units are marked (RMF: Rocky Mountains Front; SRP: Snake River Plain; YS: Yellowstone; ST: Sevier Thrust Belt; CP: Colorado Plateau; MCRS: Mid-Continental Rift System).

SED
7, 1025–1057, 2015

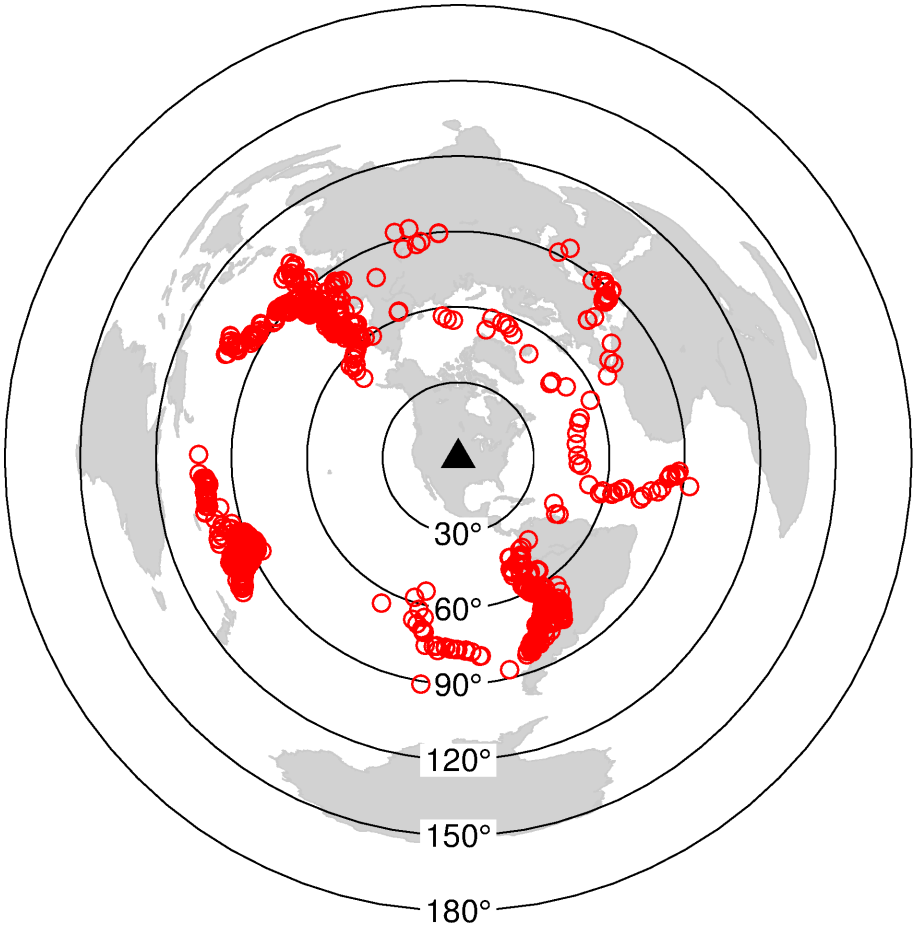

Figure 2. Epicenters of 1102 earthquakes used in our study. Black triangle marks the center of the network used. Black circles with labels indicate epicentral distances from the center.

SED
7, 1025–1057, 2015

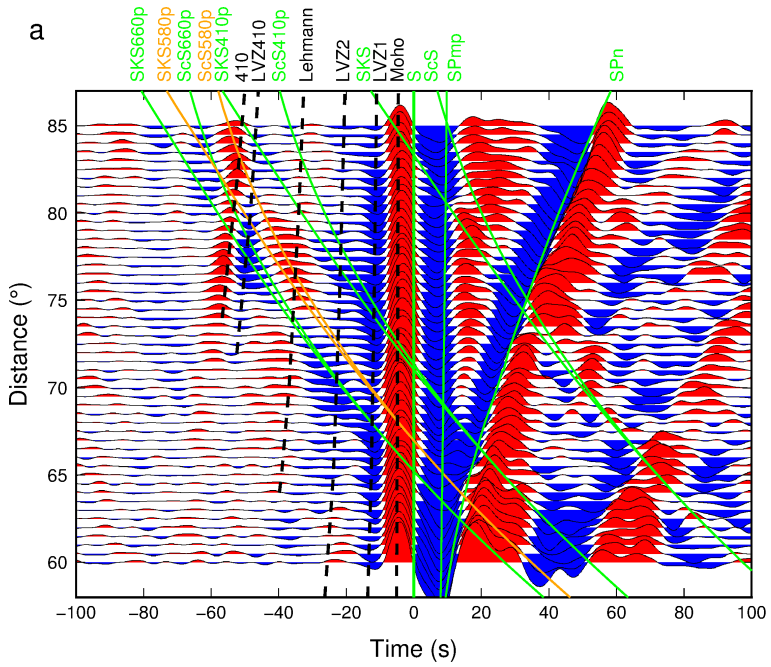

SED
7, 1025–1057, 2015

Structure of the upper mantle from USArray S-receiver functions

R. Kind et al.

Figure 3. (a) Display of binned S-receiver functions as a function of the epicentral distance. Each bin contains more than one thousand traces. Precursors of the S phase from S-to-P conversions in the upper mantle are marked with dashed black lines (410-conversion at the 410, LVZ410-conversion at a velocity reduction directly above the 410, Lehmann–Lehmann discontinuity, LVZ1, LVZ2-conversions at velocity reductions between Moho and Lehmann, Moho-conversion at the Moho). LVZ2 and Lehmann are more clear in Fig. 4, they are marked here for comparison. Additional theoretical traveltime curves of ScS, SKS, S-to-P conversions of ScS and SKS at the 410 and 660 discontinuities (ScS410p, ScS580p, ScS660p, SKS410p, SKS580p, SKS660p), crustal multiples (SPmp) and SPn are marked in green. **(b)** Ray paths of Sp, SPmp and SPn.

SED
7, 1025–1057, 2015

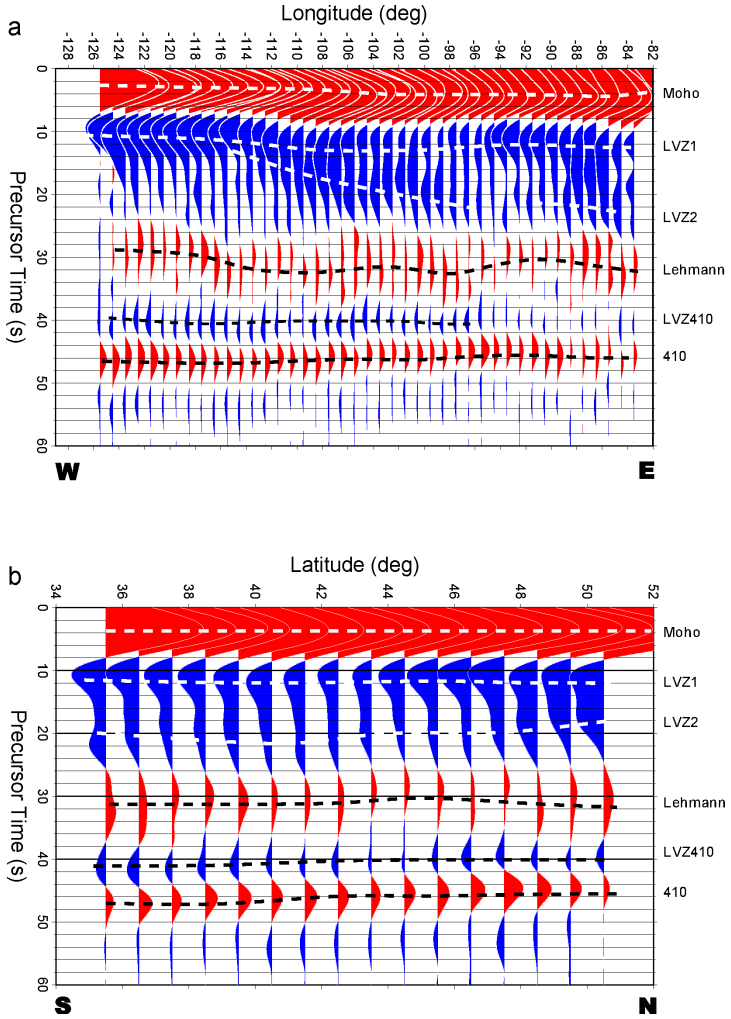

SED
7, 1025–1057, 2015

Structure of the upper mantle from USArray S-receiver functions

R. Kind et al.

Figure 4. Display of binned S-receiver function traces along a **(a)** west–east and **(b)** south–north line. LVZ1 is the LAB in the western US and the MLD in the central US. Details of LVZ1 and LVZ2 are shown in the narrower profiles in Figs. 8 and 9. "Lehmann" indicates the bottom of the asthenosphere, and LVZ410 shows a velocity drop above the 410 km discontinuity. Note that this discontinuity is only weakly observed at the eastern end of the line. "410" is the discontinuity at 410 km depth. Although these discontinuities are greatly averaged in this display, they appear very clearly.

SED
7, 1025–1057, 2015

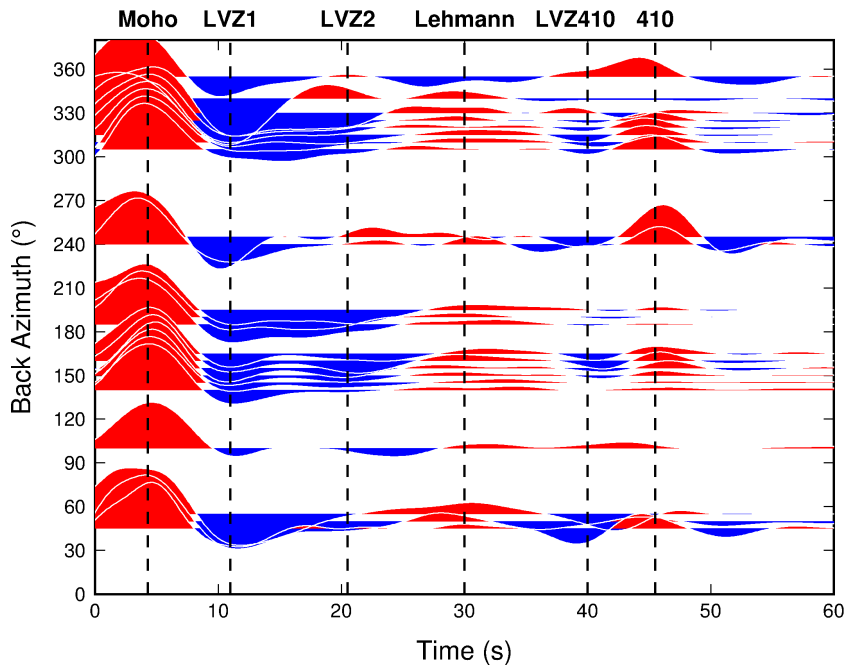

Figure 5. Display of binned S-receiver functions as a function of the backazimuth (see Fig. 2) of the source of each record, independent of epicentral distance. Only stations on the cratonic part of the US (east of 110° W) are used. The same phases as in Fig. 4 are marked. Most phases do not show any clear dependence on the backazimuth. The only exception might be the 410 discontinuity, which is strongest for sources in the northwest quadrant.

SED
7, 1025–1057, 2015

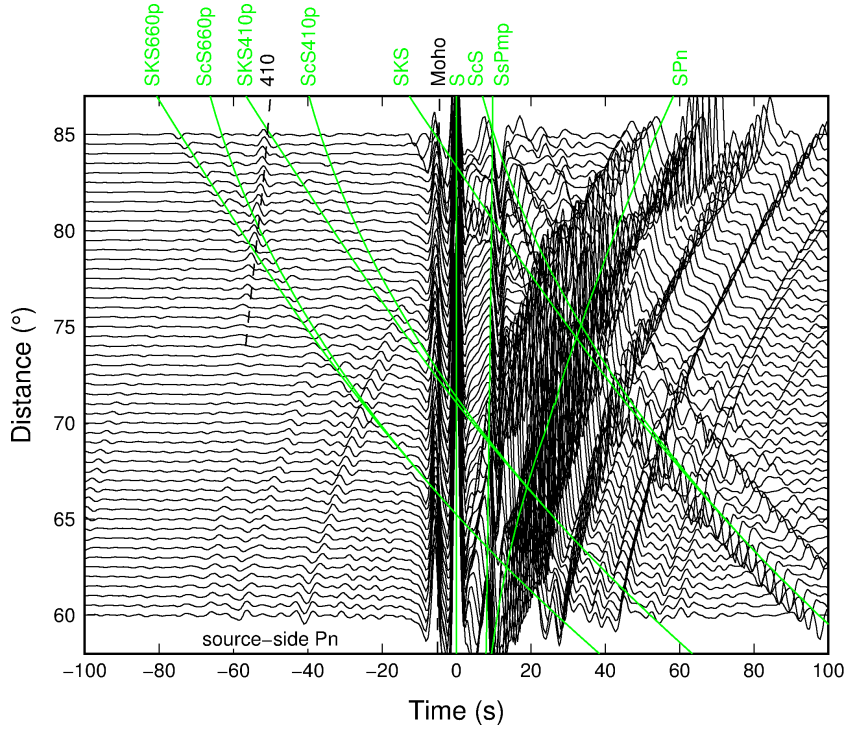

Figure 6. Theoretical seismograms (vertical component) computed with the reflectivity method for comparison with the observed data in Fig. 3a. The strong SPn phase after S agrees well with the data in Fig. 3a. A disagreement between computed and observed seismograms is the source-side Pn in front of the S signal (this figure) which is not in the data (Fig. 3a). This is a phase traveling as P along the surface on the source side and is continuously radiating S waves downward. At the receiver side these phases are converted back to P and travel again horizontally along the uppermost mantle and are observed on the vertical component. These phases are not observed in the real data probably because of heterogeneities in the real Earth.

SED
7, 1025–1057, 2015

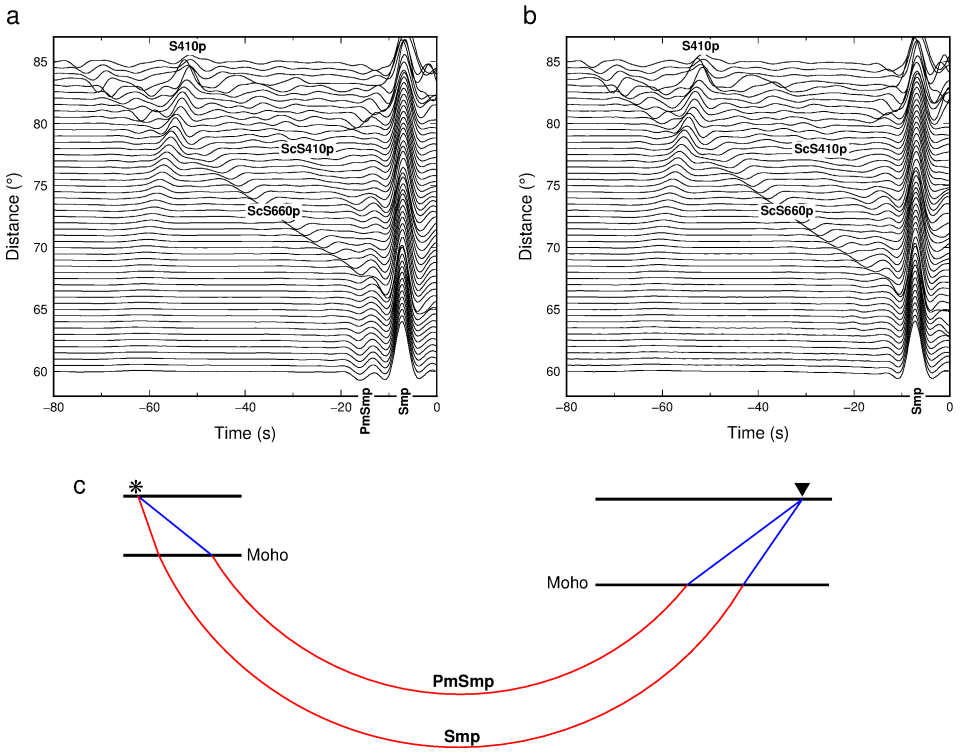

Figure 7. Theoretical seismograms for different structures at the source and receiver sides. **(a)** Moho is at 50 km depth at the source side, **(b)** no crust at the source side. Moho depth is 40 km at the receiver side in both cases. The source crust causes a negative precursor before the receiver side S-to-P conversion at the Moho (see PmSmp ray path in **(c)**), which could be mistaken as an indication of a velocity drop in the mantle below the Moho. Such phases will only be a problem in interpretations of single data traces. In receiver function processing of real data this should not be a problem since source side models and source depths are different for each record and these effects are erased by summation. **(c)** Ray paths of Smp and PmSmp.

SED
7, 1025–1057, 2015

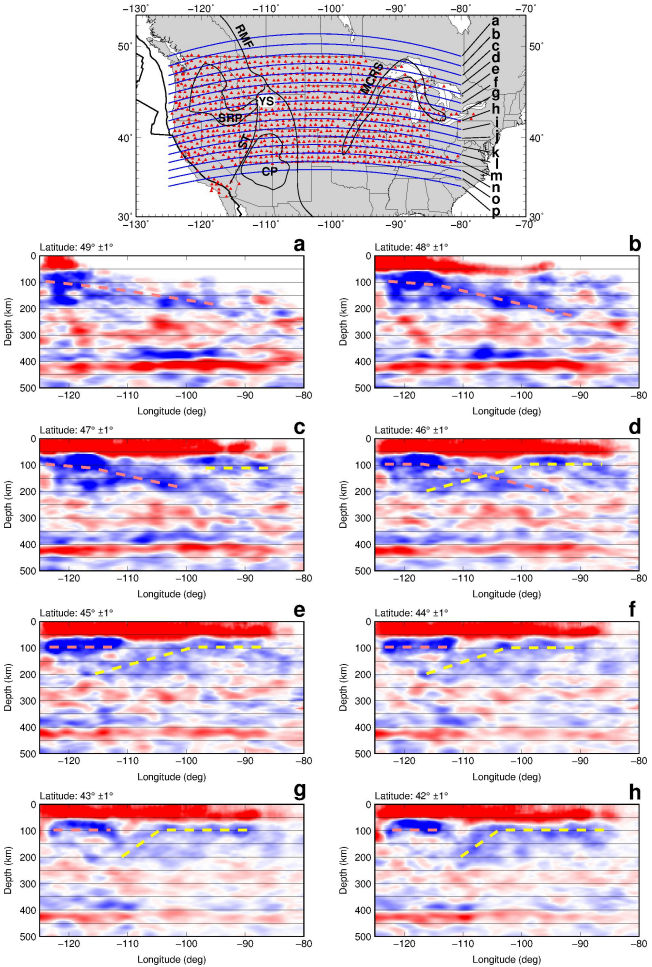

SED
7, 1025–1057, 2015

Structure of the upper mantle from USArray S-receiver functions

R. Kind et al.

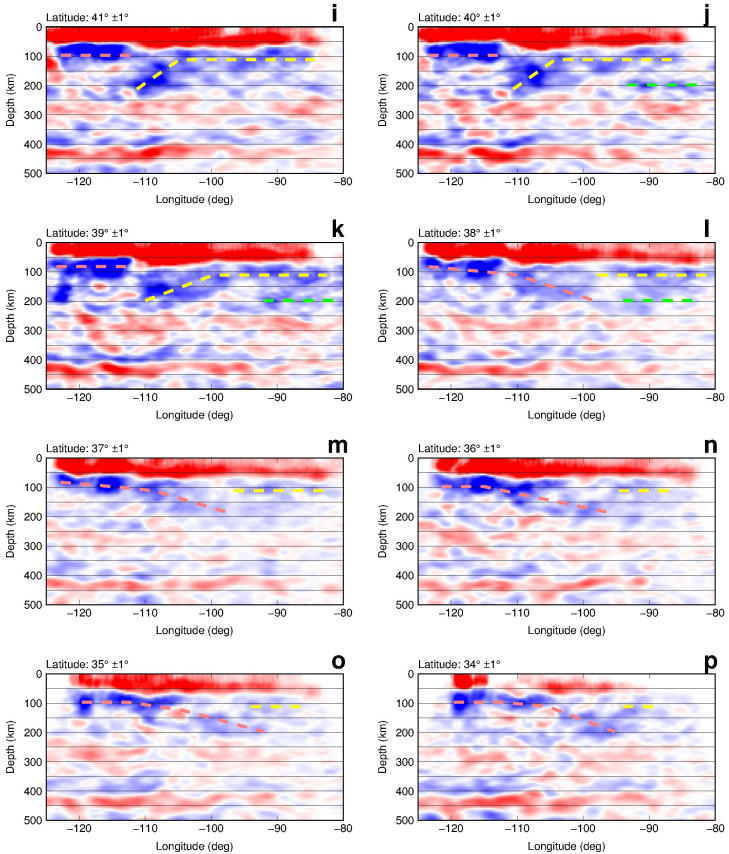

SED
7, 1025–1057, 2015

Structure of the upper mantle from USArray S-receiver functions

R. Kind et al.

Figure 8. Depth migrated west–east S-receiver function profiles (see location of the profiles at the top of the figure). Red regions at the top of each panel mark the Moho. The Moho is not the aim of the present study. Shorter period P-receiver functions are more useful for studies of the Moho. We have marked with dashed lines structures in the upper mantle which can be correlated over larger horizontal distances, although they are relatively scattered in some regions. The dashed magenta line is interpreted as LAB of the subducting Farallon plate, and the dashed yellow line as MLD of the craton. Green dashed lines **(k, l)** are indications of the cratonic LAB, which are, however, here less clear than in Fig. 4 (LVZ2). See Fig. 9 for wider profiles which show all phases clearer.

SED
7, 1025–1057, 2015

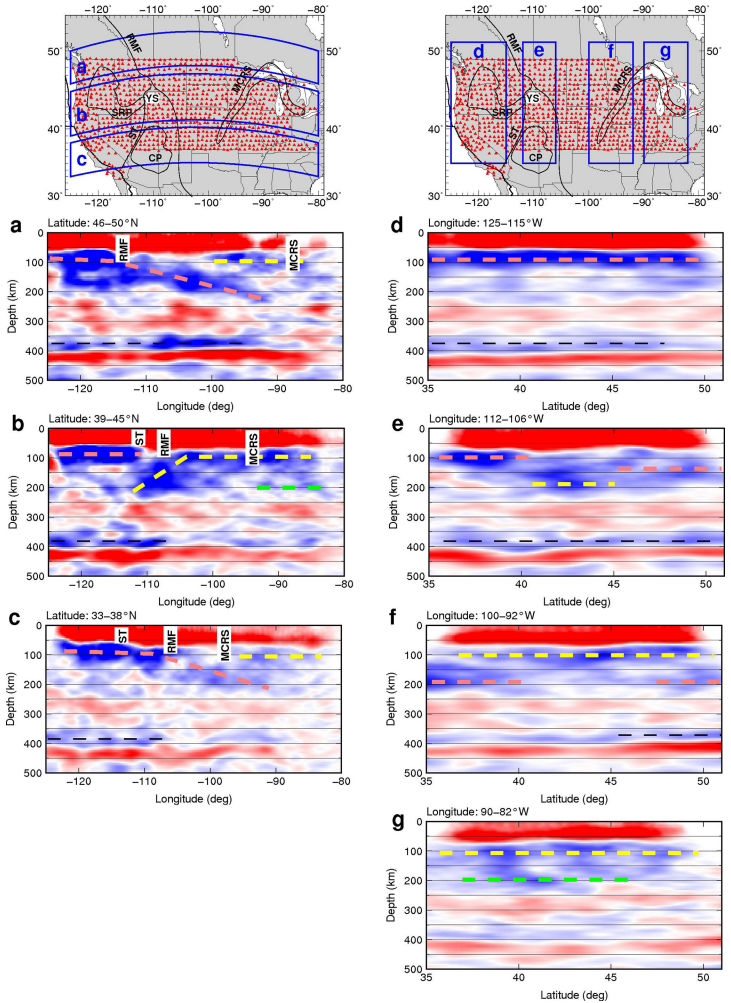

SED
7, 1025–1057, 2015

Structure of the upper mantle from USArray S-receiver functions

R. Kind et al.

Figure 9. The same data as in Fig. 8 but summed along broader south–north and west–east profiles. The profile width and orientation is shown in the location maps at the top of the figure. The LAB of the western US is marked by a dashed magenta line. The MLD is marked by a dashed yellow line. Region **(a)** (northernmost west–east profile) does not have any stations in Canada. However, due to the shallow incidence angle of the S-receiver functions, the mantle below southern Canada is also sampled by events from the northwest. The westernmost south–north profile **(d)** shows only the western LAB. In profile **(e)** we see at the southern and northern ends the western LAB, and in the central part the deep end of the MLD. In profile **(g)** we see the cratonic MLD and, weakly, the cratonic LAB (marked by a dashed green line). The cratonic LAB is also weakly visible in Fig. 8j–l. The dashed black line marks the velocity decrease above the 410 km discontinuity (LVZ410 in Figs. 3–5). There seems to be some correlation between the extent of the LAB (dashed magenta line) and the extent of the LVZ410 (dashed black line).

SED
7, 1025–1057, 2015

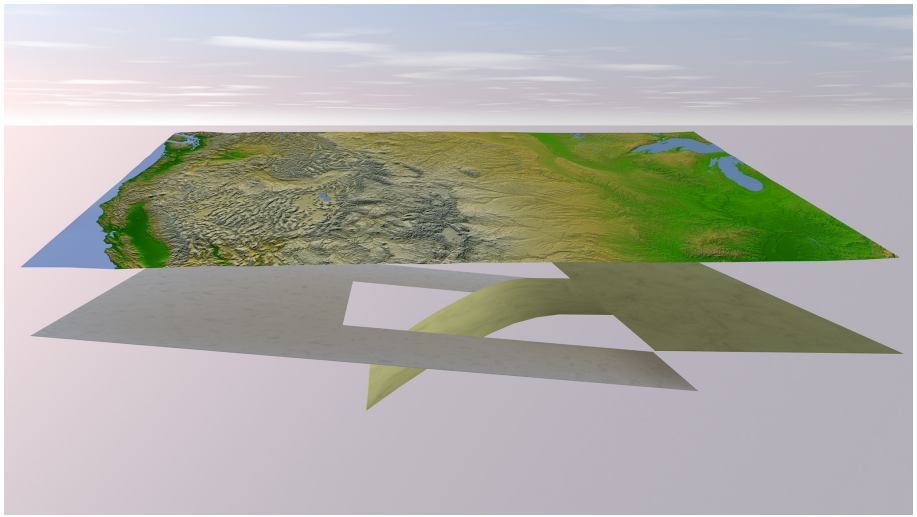

Figure 10. Visualization of the topography of the main lithospheric discontinuities in the upper 200 km in the western and central US. We see the western LAB gradually dipping in two tongues underneath the cratonic central US and the MLD of the central US plunging towards the west in between these two tongues. We interpret this complicated structure as a consequence of the collision of the Farallon and Laurentia plates.

SED
7, 1025–1057, 2015